Available online at www.sciencedirect.com

ScienceDirect

journal homepage: www.elsevier.com/locate/he

Ab initio study of lithium decoration of popgraphene and hydrogen storage capacity of the hybrid nanostructure

P. Álvarez-Zapatero [a,*], A. Herrero [a], A. Lebon [b], L.J. Gallego [c], A. Vega [a]

[a] Departamento de Física Teórica, Atómica y Óptica, Universidad de Valladolid, E–47011 Valladolid, Spain
[b] Laboratoire de Chimie Électrochimie Moléculaire et Chimie Analytique, UEB/UBO, UMR CNRS 6521, 29238 Brest Cedex, France
[c] Departamento de Física de la Materia Condensada, Facultad de Física, Universidad de Santiago de Compostela, E–15782 Santiago de Compostela, Spain

HIGHLIGHTS

- Popgraphene can be decorated in a stable way by placing Li atoms on pentagonal rings.
- The stability is due to the existence of large energy barriers for the Li diffusion.
- Closed shell interactions bond H_2 molecules to the surface.
- The average H_2-adsorption energy is 0.11 eV and the gravimetric density is 4.24 wt%.

GRAPHICAL ABSTRACT

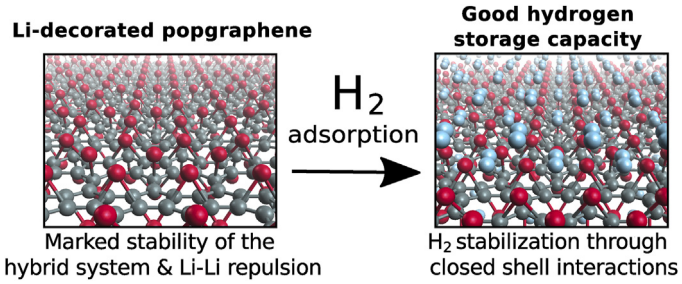

ARTICLE INFO

Article history:
Received 14 December 2020
Received in revised form
4 February 2021
Accepted 5 February 2021
Available online 11 March 2021

Keywords:
Hydrogen storage of Li-decorated popgraphene
Van der Waals-corrected DFT
Quantum-chemical topology analysis

ABSTRACT

The successful realization of extended '5-5-8' line defects in graphene in a controlled way has suggested the possible formation of a new 2D carbon allotrope consisting in pentagonal-octagonal-pentagonal carbon rings. The mechanical and thermal stability of this nanostructure, called popgraphene, has recently been confirmed on the basis of first-principles calculations. Moreover, it has been proposed as a promising anode material for use in Li-ion batteries with fast charge/discharge rates. In the present paper we perform density functional theory calculations to investigate the hydrogen storage ability of popgraphene. Our calculations show that popgraphene can be decorated in a very stable way by placing Li atoms on the pentagonal carbon rings of both sides of the sheet, leaving free the octagonal carbon rings. In that condition, the Li-decorated popgraphene sheet can bind up to four H_2 molecules per unit cell, with an average adsorption energy in a range between physisorption and atomic chemisorption, which would allow for reversible hydrogen storage at moderate temperatures and pressures. Moreover, the gravimetric density of the Li-decorated popgraphene is 4.24 wt%, which is almost equal to the threshold specified by the U.S. Department of Energy for novel hydrogen-storage materials. All these results show

* Corresponding author.
E-mail address: pablo.alvarez.zapatero@uva.es (P. Álvarez-Zapatero).
https://doi.org/10.1016/j.ijhydene.2021.02.058

that Li-decorated popgraphene nanostructures could be good materials for hydrogen storage.

Introduction

The aim of the 'hydrogen economy' [1–7] is the use of hydrogen (an abundant and clean energy source) as fuel, but there are still numerous technical challenges for its implementation at a large-scale. In particular, only some companies offer today models of hydrogen cars, and they are still quite expensive compared to traditional fossil fuel cars. Buses, trains, canal boats, ships and aeroplanes are other examples of transport vehicles that can already run with hydrogen in various forms. The extensive use of hydrogen vehicles, with complementary energy alternatives such a metal-ion batteries, could contribute to phase out fossil fuels and limit global warming.

A critical problem for the use of hydrogen in on-board automotive applications is hydrogen storage. The conventional hydrogen storage by high-pressure tanks has considerable risks and other inconveniences, and in the last decades other possibilities have been explored. In particular, theoretical studies have been performed to investigate the hydrogen storage ability of carbon nanostructures such as carbon nanotubes [8,9], graphene [10,11], pillaraded graphene [12], sandwiched graphene-fullerene composites [13] and graphene slites pores [14], the latter of which can be considered as simple models for the pores existing in nanoporous carbon materials such as activated carbons [15] and carbide-derived carbons [16]. Experimental studies have been performed on several carbon nanostructures such as single-walled carbon nanotubes (SWCNTs) [17], nanoporous spongy graphene [18], few-layer graphene-like flakes [19] and nanoporous activated carbon cloths [20], among others.

There are well-defined requirements for a material to be a good candidate for hydrogen storage, i.e., to be used in hydrogen-powered vehicles with the same autonomy range as that of the gasoline ones. Two of the main conditions set by the U.S. Department of Energy (DOE) for novel hydrogen-storage materials are a good gravimetric density of at least 4.5 wt% and an adsorption energy in a range between physisorption and atomic chemisorption, which would allow storage and discharge to be cycled at ambient conditions [21–24]. In general, the studies performed so far on carbon nanotubes and graphene-based systems have shown that in pristine form they do not fulfil the H_2-adsorption energy criterion. However, it has been shown that these nanostructures could be used as hydrogen storage media if they are doped or decorated with atoms of carefully selected species such as early transition metals and alkali and alkali-earth metals, which have not clustering tendency on those substrates. For instance, Yildirim and Ciraci [25] have performed density-functional-theory (DFT) calculations with the generalized gradient approximation (GGA) to show that the hydrogen-storage capacity of Ti-decorated SWCNTs is high. A similar conclusion has been obtained by Lebon et al. for Ti-decorated zigzag graphene nanoribbons by means of van der Waals (vdW)-corrected DFT calculations [26]. Metal decoration has also been used to increase the hydrogen storage capacity of non-carbon nanostructures, such as phosphorene [27–30] and borophene [31–34].

Among the numerous 2D materials of the post-graphene era (many of them not synthesized yet), a number of novel 2D carbon allotropes have been proposed with many potential applications, such as penta-graphene [35], phagraphene [36], Ψ-graphene [37], and phographene [38]. Recently, a new 2D carbon allotrope has been proposed on the basis of first-principle calculations. It consists in pentagonal-octagonal-pentagonal carbon rings, and it has accordingly named popgraphene [39]. The theoretical prediction of popgraphene was preceded by a study describing the realization of highly regular '5-5-8' line defects in graphene by means of simultaneous electron irradiation and Joule heating [40]. Popgraphene is metallic and has great mechanical and thermal stability. Moreover, it has been predicted to have a high capacity for Li atoms, a low Li diffusion barrier, and a low average open circuit voltage [39]. These characteristics suggest that popgraphene could be a promising anode material for use in Li-ion batteries with fast charge/discharge rates.

Motivated by those findings, in the present paper we explore the potential application of popgraphene as a hydrogen storage medium after Li decoration, something that to our knowledge has not been performed yet. Our aim was twofold: firstly, we wished to construct a stable Li-decorated popgraphene framework suitable for H_2 adsorption, and secondly we wanted to investigate the largest number of H_2 molecules that can be bound to such Li-decorated nanostructure. Besides the structural and energetic aspects, our investigation includes a careful analysis of the stability of the Li/popgraphene structure that is based on estimating the energy diffusion barriers of the Li atoms, and a study of the charge distributions of the Li/popgraphene and Li/popgraphene + H_2 systems. As it will be seen, the results presented in this paper provide a complete understanding of the Li adsorption mechanisms on popgraphene.

The essential technical details of the computational method used in this work are described in the next section. The following sections are devoted to the presentation and discussion of our results, and in the final part we summarize our main conclusions.

Computational details and theoretical background

The calculations were performed with the Vienna ab initio simulation package (VASP) [41,42], which solves the Kohn-

Sham equations within the DFT using plane waves as basis set to expand the wave function. A cut-off energy of 700 eV was used for the plane-wave basis. Exchange and correlation effects were described at the GGA level as implemented in the PBE functional [43], and corrections due to vdW forces were included using the Grimme D2 approximation [44]. The core interactions were treated within the projector-augmented wave (PAW) approach [45], and the considered active valence spaces were 1s for H, 2s2p for C, and 1s2s for Li. Periodic images of the sheet along the normal to its surface were separated by a distance of 20 Å after a careful convergence check. A k-grid of 13 × 13 × 1 was used for integrating in the Brillouin zone. Methfessel-Paxton [46] at second order and Gaussian smearings were used with a smearing width of 0.1 eV and 0.05 eV, respectively. Structural relaxations were performed until the total force remaining on each atom was smaller than 0.01 eV/Å and the external pressure was minimal. The electronic convergence criterion used for total energies was 10^{-4} eV/unit cell.

After the structural information obtained with VASP, it is natural to inquire into the way in which the components of the system hold together. This can be done by means of a quantum chemical topology analysis. This approach analyses different relevant scalar fields that are often discussed in the literature, such as the electronic density and the electron localization function (ELF), among others [47]. For practical reasons, we will restrict our analysis to the more intuitive electronic density. The nature of the bonding can be elucidated from the analysis of the critical points of this density. In the following, bond critical points and ring critical points will be denoted as BCPs and RCPs, respectively. BCPs are saddle points of the electronic density exhibiting a minimum of the density along the bond path that connects two atoms; they also present two maxima in directions normal to this path. RCPs are second species saddle points that are encountered in cyclic environments. Whatever the line within the plane of the cycle, it is minimum at the RCP. The RCP displays however a maximum of density in a direction normal to the plane of the cycle. These RCPs are usually encountered in the analysis of compounds having aromatic cycles [48,49] or they appear during the closing of a cycle in a chemical reaction [50]. According to the value of the density, the Laplacian of the density or the energy at the BCPs, it is possible to discriminate between covalent, ionic, polar, dative, metallic, vdW or hydrogen bonds [51,52]. The atomic units of those quantities are respectively $e.Bohr^{-3}$, $e.Bohr^{-5}$ and $Ha.Bohr^{-3}$, and we shall refer to them with the common symbol a.u. Matta [52] ranges the bonds between the share and close shell bonds. The former are the covalent, polar-covalent bonds; among the latter there are the dative, ionic, metallic and vdW bonds. To fix the idea, a typical covalent bond displays a value of the electronic density at the BCPs superior to 0.2 a.u and a negative Laplacian comprised between −0.5 and −1.0 a.u. The negative Laplacian testifies an accumulation of electronic density in the BCP region. An ionic bond displays a much weaker value of the electronic density at the BCPs, typically one order of magnitude lower than that of a covalent bond, and a positive Laplacian is suggestive of a charge depletion (≈0.1 − 0.2 a.u.). More details can be found in the paper of Matta [52], where dative, vdW and metallic bonds are also alluded. The energy at the BCPs can also be computed and it is generally negative for a covalent bond whereas it is positive for an ionic bond.

In the present study, 2 × 2 replica of the optimized VASP cells were prepared and all-electron single-point energy calculations were performed on these replica with the well-stablished quantum chemistry code Gaussian16 [53] at the same level of theory and with a 3-21G* basis set. In fact, PAW or pseudopotentials usually introduce a smoothing of the electron density at the cut-off radius. As the analysis of this scalar field relies on the use of the mathematical gradient, it might add some spurious minima around a sphere whose radius is the cut-off radius [54]. Hence, it is recommended to use scalar fields produced by all-electron codes. The derived wavefunction is an input for building the electronic density with which BCPs and RCPs are extracted after an analysis with the DGRID5.1 code [55]. It was also possible to compute the electronic populations on atoms with DGRID5.1, that integrates the charge over the atomic basins.

Li-decorated popgraphene

Fig. 1 shows a schematic representation of the popgraphene structure. The unit cell contains 12 C atoms, with C atoms occupying two types of non-equivalent atomic positions, denoted as C1 and C2, and its plane group is c2mm. The predicted lattice constants are 3.69 Å and 9.10 Å, and the bond lengths C_1–C_2 and C_2–C_2 of the same pentagon are 1.44 Å and 1.46 Å, respectively, while the C_1–C_1 and C_2–C_2 bonds belonging to the same octagon have a length of 1.40 Å. All these structural results agree quite well with those reported by Wang et al. [39]. The cohesive energy of popgraphene is 7.69 eV. The cohesive energies are defined, in general, as $E_c = (\sum_i E_i - E_T)/n$, where E_T is the total energy of the system per unit cell and E_i are the energies of the free n atoms in that cell. By definition $E_c > 0$ indicates binding, and the higher E_c, the stronger is the binding.

As mentioned above, one of our main objectives in this paper is to decorate the popgraphene sheet with Li atoms in a stable and appropriate way to be latter used as supporting framework for investigating the adsorption of H_2 molecules. Accordingly, we successively added Li atoms to the popgraphene sheet and relaxed the hybrid nanostructures. Fig. 2 shows the relaxed structures of popgraphene after deposition of a single Li atom on pentagonal and octagonal hollow sites, the most stable adsorption sites. The cohesive energies and bond distances from the Li atom to the sheet are, respectively, 7.25 eV, 1.70 Å, and 7.26 eV, 1.30 Å (the octagonal hollow site is therefore energetically more favourable, in keeping with the prediction by Wang et al. [39]), and the formation energies are 1.97 eV and 2.08 eV, respectively. The formation energies were calculated using the general expression $E_f = [E(PG) + nE(Li) - E(PG + nLi)]/n$, where $E(PG)$, $E(Li)$ and $E(PG + nLi)$ are the energies of pristine popgraphene, that of a single Li atom, and that of the optimized structure of popgraphene upon adsorption of n Li atoms. It can be seen that the Li doping of popgraphene is an exothermic process.

In the addition of more Li atoms to the popgraphene sheet, we exploited the symmetry conditions and considered only

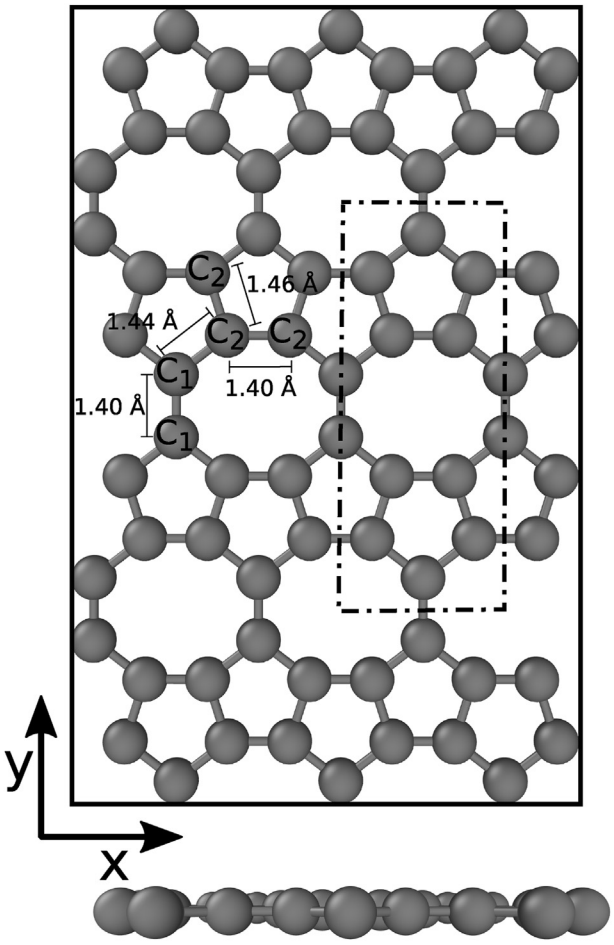

Fig. 1 – Top and side views of the relaxed structure of popgraphene, showing the non-equivalent carbon atoms C_1 and C_2. The C atoms are plotted as dark grey balls. The unit cell is represented by a dashed rectangle.

even numbers of Li atoms, examining in each case several initial candidates for structural optimization. In particular, for $n = 2$ we considered fourteen arrangements of the Li atoms on pentagonal and/or octagonal hollow sites of the same and different sides of the sheet. All the structures obtained upon relaxation are shown in Fig. S1 of the Supporting Information (SI), and Table S1 lists their cohesive energies and formation energies. The relaxed structures show a preference of the Li atoms to be separated, being more stable when those atoms are on opposite sides of the sheet. The most stable structure, shown in Fig. 2, corresponds to that in which the two Li atoms are on octagonal hollow sites of different sides of the sheet. The bonding distance from the Li atoms to the sheet is 1.25 Å, and the structure shows a slight bending due to the presence of these atoms.

For $n = 4$, we considered seven arrangements of the Li atoms on pentagonal and/or octagonal hollow sites of the same and different sides of the sheet (see Fig. S2 and Table S2). The most stable structure, shown in Fig. 2, has all the Li atoms on pentagonal hollow sites on both sides of the sheet, at 1.75 Å from the surface. As in the previous case, the relaxed structures have a clear preference for large Li–Li distances, the least favourable being that with all Li atoms on pentagonal hollow sites on the same side of the sheet.

Finally, for $n = 6$ we considered nine arrangements of the Li atoms on pentagonal and/or octagonal hollow sites of the same and different sides of the sheet (see Fig. S3 and Table S3), including a configuration proposed by Wang et al. [39] in which the six Li atoms cover the pentagonal and octagonal hollow sites of one side of the unit cell of the sheet. The most stable structure, shown in Fig. 2, is equal to the most stable structure obtained in the case of four Li atoms plus two Li atoms placed at bridge positions between adjacent octagonal rings at 2.00 Å from the surface, leaving free the octagonal hollow sites. The bridge positions become stable in order to enlarge the Li–Li distances and, again, the popgraphene sheet is slightly bended due to the presence of the Li atoms. It is this the structure (named henceforth simply as 6Li/PG) that will be used as supporting framework for the adsorption of H_2 molecules. The reason is that it is a very stable structure in which both sides are equivalent, and leaves a wide free space for hydrogen adsorption while having enough Li atoms to bond the H_2 molecules. We note that the configuration proposed by Wang et al. [39] for popgraphene decorated on one side with six Li atoms (per unit cell) placed on pentagonal and octagonal hollow sites is not the most stable one. Our calculations show that such configuration is indeed reached after relaxation if the Li atoms are initially placed on those hollow sites but not far from the popgraphene surface. However, when the Li atoms are initially placed on the same hollow sites but at a longer distance from the popgraphene surface, the relaxation of the system leads to a configuration in which only the four Li atoms that are on pentagonal hollow sites are located close to the popgraphene surface, while the other two Li atoms (those which are on octagonal hollow sites) remain far away from the surface, although bonded to the sheet. These metastable and stable structures are shown in Fig. 3; the shortest distance between Li atoms located at pentagonal and octagonal hollow sites in the metastable structure is 2.52 Å, while in the stable structure is 3.07 Å. In fact, what our previous results show is that there is a general trend of the Li atoms to be separated on the popgraphene surface, suggesting that they acquire a positive charge due to a charge transference to the popgraphene substrate, in a similar fashion to what occurs when Li atoms are deposited on graphene [56]. The electron charge redistribution in the particular but representative case of the 6Li/PG system will be discussed in detail in the Quantum chemical topological analysis section.

Besides the structural and energetic characteristics, the mobility of the Li atoms on the popgraphene surface is an important factor to be taken into account when analysing the ability of this material for hydrogen storage. We note, for instance, that this factor explains why Ca-decorated graphene-based nanostructures, which were early proposed as appropriated media for H_2 storage on the basis of the low cohesive energy of bulk Ca, do not satisfy the necessary requirements for that purpose. In fact, DFT studies on the migration energy of Ca atoms on the graphene surface show that the diffusion barrier is as small as 0.07 eV, which allows the Ca atoms to move easily on the graphene surface and form clusters [57]. In contrast, the energy barrier of the slightly heavier Ti atom is one order of magnitude higher, 0.60 eV [57], which contributes to the good ability of Ti-decorated graphene-based nanostructure for hydrogen storage [25,26].

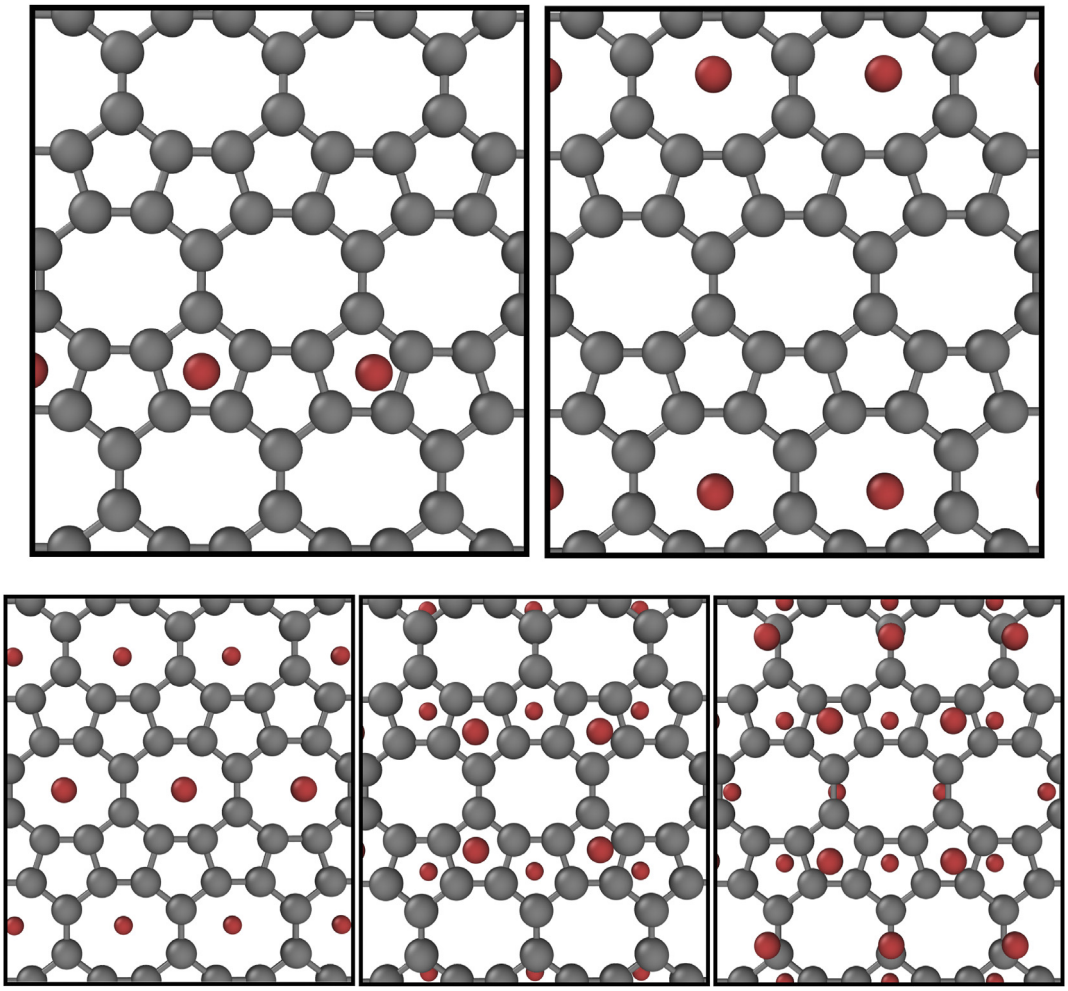

Fig. 2 – Relaxed structures of popgraphene with a single Li atom on the pentagonal and octagonal hollow sites (upper panels), and the most stables structures of the *n*Li/popgraphene systems ($n = 2, 4, 6$) (lower panels). The C and Li atoms are plotted as dark grey balls and red balls, respectively. The Li atoms on the front side have a greater size than the Li atoms on the rear side. (For interpretation of the references to color in this figure legend, the reader is referred to the Web version of this article.)

Wang et al. [39] have calculated the diffusion barriers of a Li atom on pristine popgraphene by considering four paths, connecting hollow sites of the popgraphene surface, for the movement of the Li atom. We have performed similar calculations, and the results are shown in Fig. 4. Our calculations were carried out by relaxing the distance from the Li atom to the popgraphene sheet along each path, keeping fixed the rest of the system. The energetic pictures associated to the four diffusion paths are shown in the right panel of Fig. 4. The energy profiles for the diffusion of the Li atom on the popgraphene surface along the paths are consistent with the results obtained by Wang et al. [39]. It can be seen that the energy barriers to escape from an octagonal hollow site are above 0.4 eV, while the movement from pentagon to pentagon is easier, although the energy barrier is above 0.3 eV. These energy barriers are significant and sufficient to quench the Li mobility on the popgraphene layer at moderate temperatures, since room temperature corresponds to about 0.025 eV. Once the Li atom falls into an octagonal site, the energy barriers would prevent any further displacement of the atom on the surface.

When more Li atoms are adsorbed on the popgraphene layer, the energy barriers are dramatically increased, which restricts the movement of the Li atoms (upon moderate thermal excitations) to positions close to their equilibrium positions. We analyse in detail this phenomenon to further explain the marked stability of the 6Li/PG structure (Fig. 2). Figs. 5 and 6 show the diffusion paths of Li atoms of the system 6Li/PG with starting positions at octagonal and pentagonal hollow sites, respectively. The energy profiles of the diffusion paths are shown in the right panels of those figures. In particular, the right panel of Fig. 5 shows that the diffusion of the Li atom from an octagonal hollow site to a bridge site between two pentagonal carbon rings is energetically very favourable (at this position there is an energy drop of 0.3 eV), which is consistent with the equilibrium positions of two of the Li atoms (one on each side) of the 6Li/PG structure (see Fig. 2). However, the movement of the Li atom from an

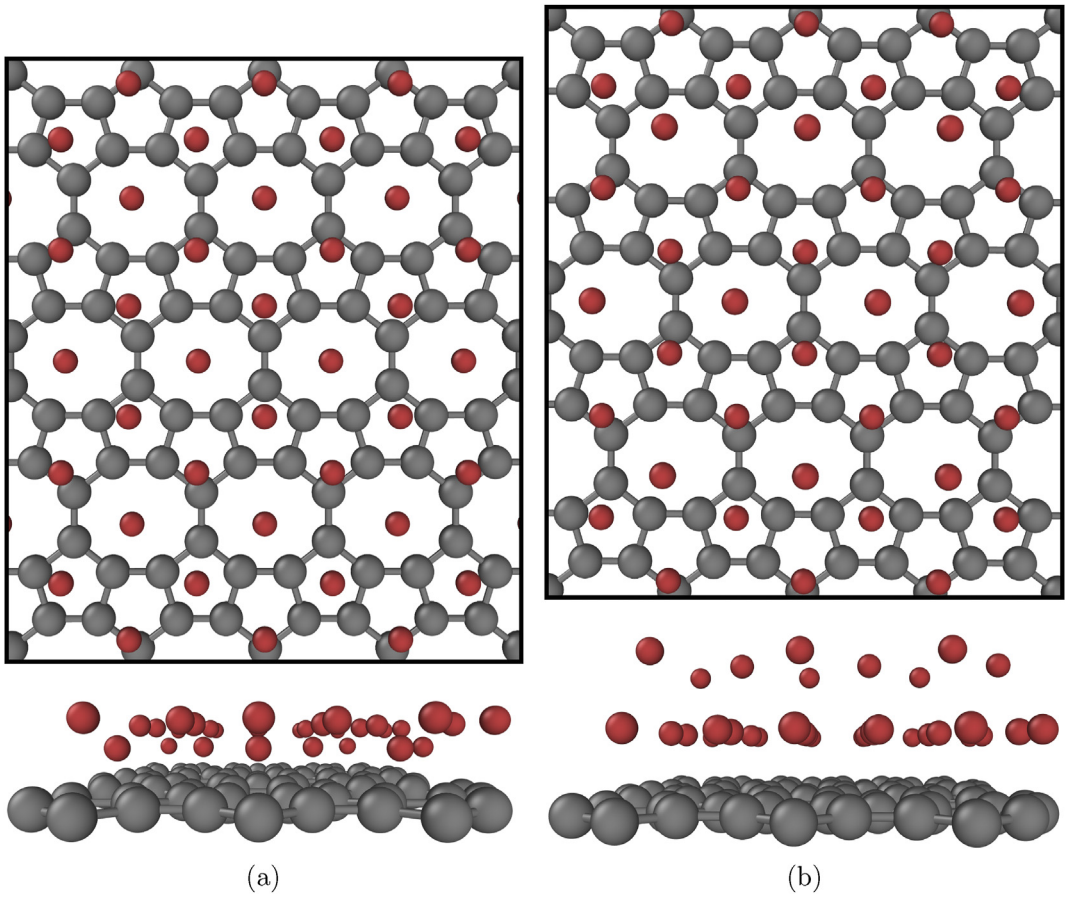

Fig. 3 – Top and side views of the relaxed structures of popgraphene decorated on one side with Li atoms at the pentagonal and octagonal hollow sites, when the Li atoms are initially placed near the popgraphene surface (left) and when they are placed far from the popgraphene surface (right). The C and Li atoms are plotted as dark grey balls and red balls, respectively. Note that the portions of the popgraphene layer used in this figure have not the same size than those used in Fig. 2. (For interpretation of the references to color in this figure legend, the reader is referred to the Web version of this article.)

octagonal hollow site to a pentagonal hollow site (path 2 in Fig. 5) is quite unfavourable: the energy barrier is over 1.0 eV, and the final position is indeed not an equilibrium position. On the other hand, the diffusion of the Li atom starting from a pentagonal hollow site (Fig. 6) involves an energy barrier of about 2.0 eV and another of more than 3.0 eV. It can therefore be concluded that the marked stability of the 6Li/PG structure is connected to the existence of large energy barriers for the diffusion of the Li atoms, which block their movements around the equilibrium positions. It should be pointed out that calculation of the energy of a system composed by a cluster of six Li atoms deposited on popgraphene yields a value much bigger than that of the 6Li/PG structure, which is a direct proof that Li clustering on the popgraphene surface is an energetically very unfavourable process.

It can be seen in Fig. 6 that the path 2 shows a deep minimum over the bridge between an octagonal ring and a pentagonal ring. This is a consequence of the fact that, at this position, the Li atom has been expelled from the popgraphene surface as a consequence of Li–Li interactions. It should be born in mind that in the determination of the energetic profiles for the diffusion of a Li atom in the 6Li/PG system along the popgraphene surface, other Li atoms are already present on the sheet, and at some positions they can push up the moving Li atom. Thus, at these configurations the moving Li atom has a larger bond distance to the popgraphene sheet in order to lower the Li–Li repulsion, being more stable than its neighbouring configurations along the path, since the energy barriers are now mainly driven by the Li–Li interactions.

Hydrogen adsorption on Li-decorated popgraphene

Using now as host material the very stable 6Li/PG structure, we investigated its ability for hydrogen adsorption by successively adding H_2 molecules to this system. In the case of a single adsorbed H_2 molecule, we considered a fair number of starting configurations (a configuration is a combination of site and orientation of the H_2 molecule). The relaxed structures of all the systems with H_2-adsorption energies in the range 0.1–0.3 eV are shown in Fig. S4 of the SI, and Table S4 shows their H_2-adsorption energies. These energies were computed using the general expression $E_a = [E\ (6Li/PG) + nE\ (H_2) - E\ (6Li/PG + nH_2)]/n$, where $E\ (6Li/PG)$ and $E\ (6Li/PG + nH_2)$ are the energies of the 6Li/PG structure and that of the

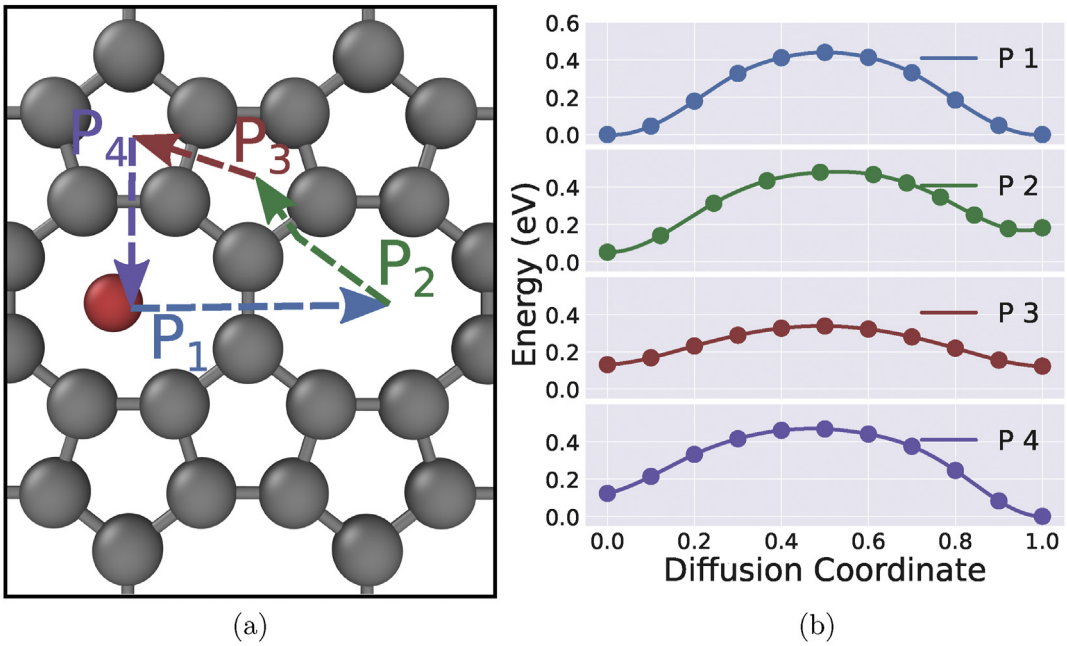

Fig. 4 – Diffusion paths for the movement of a single Li atom on the popgraphene surface (left) and their corresponding energy profiles (right). The C atoms and the Li atom are plotted as dark grey balls and red ball, respectively. (For interpretation of the references to color in this figure legend, the reader is referred to the Web version of this article.)

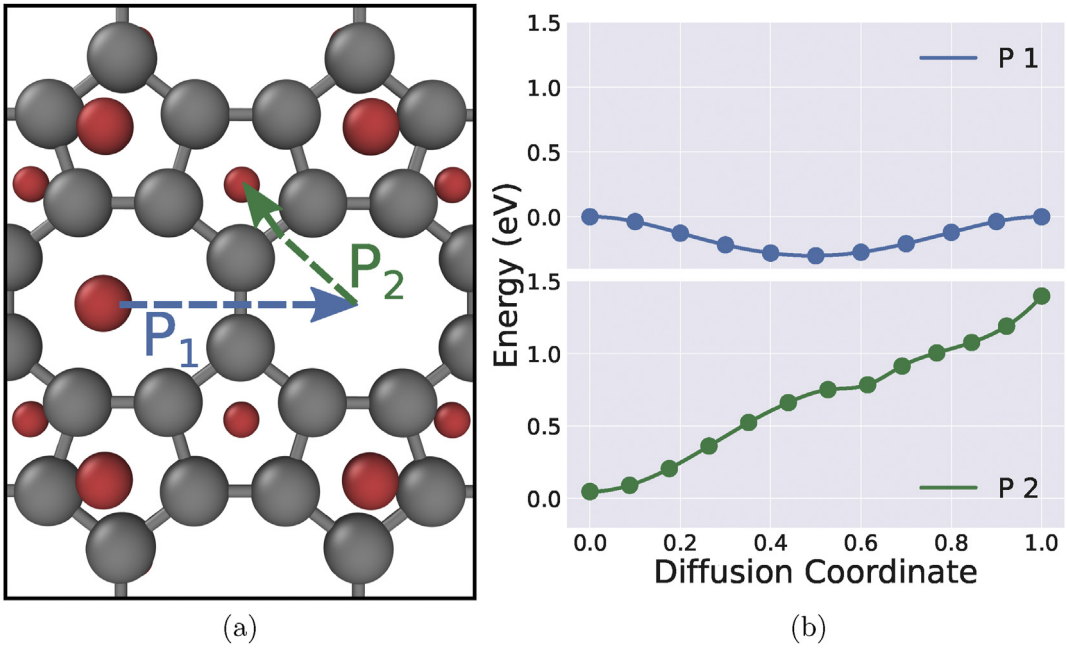

Fig. 5 – Diffusion paths for the movement of a Li atom of the 6Li/PG system on the popgraphene surface, starting from an octagonal hollow site (left), and their corresponding energy profiles (right). The C and Li atoms are plotted as dark grey balls and red balls, respectively. The Li atoms on the front side have a greater size than the Li atoms on the rear side. (For interpretation of the references to color in this figure legend, the reader is referred to the Web version of this article.)

structure obtained upon adsorption of n H_2 molecules. The most stable structure of the 6Li/PG + H_2 system is shown in Fig. 7. In that configuration, the H_2 molecule is situated on an octagonal hollow site at 3.00 Å from the popgraphene layer, while the neighbouring Li atoms, located at pentagonal hollow sites, are at 2.90 Å from the H_2 molecule. The H_2-adsorption energy is 0.15 eV, but the gravimetric density is 1.07 wt%, much lower than the DOE target of 4.5 wt%. We note that there is a high degree of energetic degeneracy in the possible configurations of the system 6Li/PG + H_2 shown in Fig. S4 (see Table S4), all of them having the H_2 molecule in the surroundings of an octagonal hollow site.

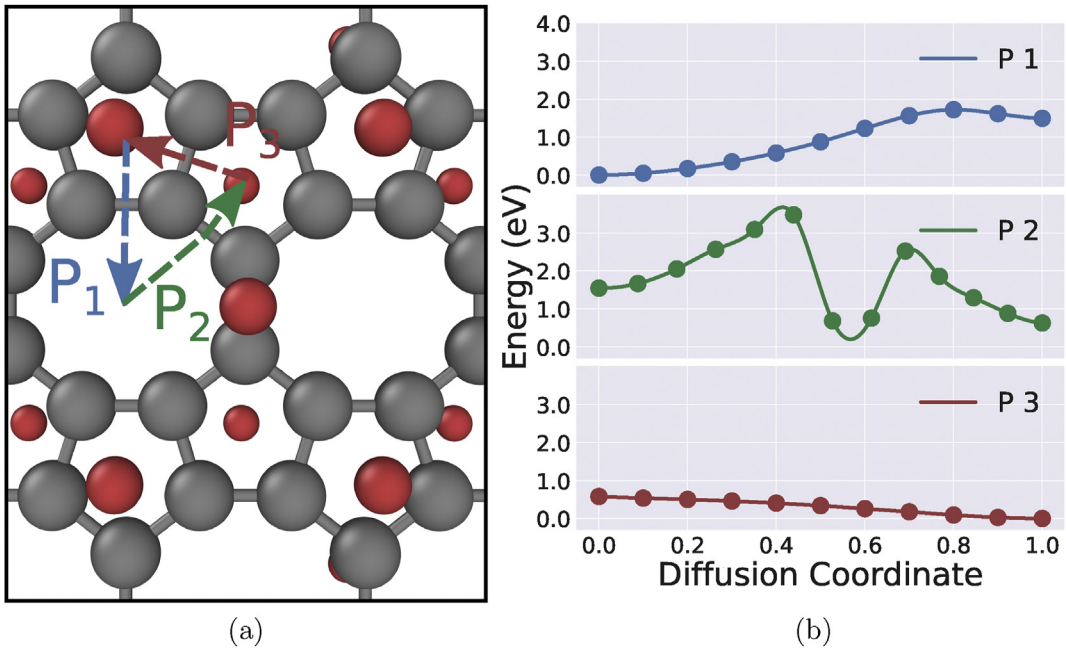

Fig. 6 – Diffusion paths for the movement of a Li atom of the 6Li/PG system on the popgraphene surface, starting from a pentagonal hollow site (left), and their corresponding energy profiles (right). The C and Li atoms are plotted as dark grey balls and red balls, respectively. The Li atoms on the front side have a greater size than the Li atoms on the rear side. (For interpretation of the references to color in this figure legend, the reader is referred to the Web version of this article.)

By adding H_2 molecules to the most stable 6Li/PG + H_2 structure, we computed the most stable configurations of the systems 6Li/PG + nH_2 ($n = 2–5$), and the results are shown in Fig. 7. In Fig. S5 and Table S5 we give information on the structures of all the systems that were found to have H_2-adsorption energies in the range 0.1–0.3 eV. We discuss each case in detail below.

For 6Li/PG + $2H_2$, we only investigated one structural candidate, the natural choice inferred by symmetry conditions from the result obtained for 6Li/PG + H_2, i.e., the 6Li/PG + H_2 system plus an extra H_2 molecule situated on the same octagonal hollow site as the already adsorbed H_2 molecule, but in the rear side of the popgraphene sheet. In the relaxed configuration, the average H_2-adsorption energy of the system 6Li/PG + $2H_2$ is 0.13 eV, and the gravimetric density is 2.12 wt%, still lower than the DOE threshold of 4.5 wt%.

For 6Li/PG + $3H_2$, the most stable structure was that of the system 6Li/PG + $2H_2$ plus an extra H_2 molecule placed over a Li atom adsorbed on a pentagonal hollow site (at 3.00 Å from it), close to another H_2 molecule (at 2.90 Å) (see Fig. 7). Thus, the extra H_2 molecule interacts both with the Li atom and another H_2 molecule. The H_2-adsorption energy of the system 6Li/PG + $3H_2$, is 0.12 eV, with a gravimetric density of 3.15 wt%. In Fig. S5 we show two other possible candidates that were found for the system 6Li/PG + $3H_2$, with similar H_2-adsorption energies (see Table S5). In the first one, the extra H_2 molecule is a little farther from the popgraphene layer, while in the other the extra H_2 molecule is on an octagonal hollow site, vertically positioned, and far from other H_2 molecules and from the neighbouring Li atoms. Note that in the most stable configuration of 6Li/PG + $3H_2$, the extra H_2 molecule is close both to a Li atom and another H_2 molecule, thus reflecting the role played by the dopant Li atoms in the hydrogen adsorption on the system.

Similarly, the most stable configuration of 6Li/PG + $4H_2$ has the fourth H_2 molecule close to the previously introduced H_2 molecule, but on the rear side of the popgraphene sheet. The second most stable configuration (see Fig. S5 and Table S5) is similar, although with a larger distance between the H_2 molecules and the Li atoms. The H_2-adsorption energy of the most stable configuration of 6Li/PG + $4H_2$ is 0.10 eV, with a gravimetric density of 4.24 wt%, very close to the DOE target of 4.5 wt%. Finally, the H_2-adsorption energy of the most stable structure of 6Li/PG + $5H_2$ decreases to 0.09 eV (although the gravimetric density reaches 5.15 wt%), a value that is in the limit for allowing reversible hydrogen storage. In that configuration, the fifth H_2 molecule is located on an octagonal hollow site (see Fig. 7). We can therefore conclude that the maximum number of H_2 molecules that can be attached to the system 6Li/PG per unit cell satisfying the H_2-adsorption energy criterion for reversible storage is four, and that in such situation the system has an efficient gravimetric density of more than 4 wt%.

Quantum chemical topological analysis

Li decoration of popgraphene on one side

We first discuss the results of the quantum chemical topological analysis of the metastable and stable structures shown in Fig. 3. In Fig. 8 we show again these two structures. In the metastable structure (upper panels of Fig. 8), most of the bonds involving Li atoms are Li–C bonds, the DGRID5.1 code

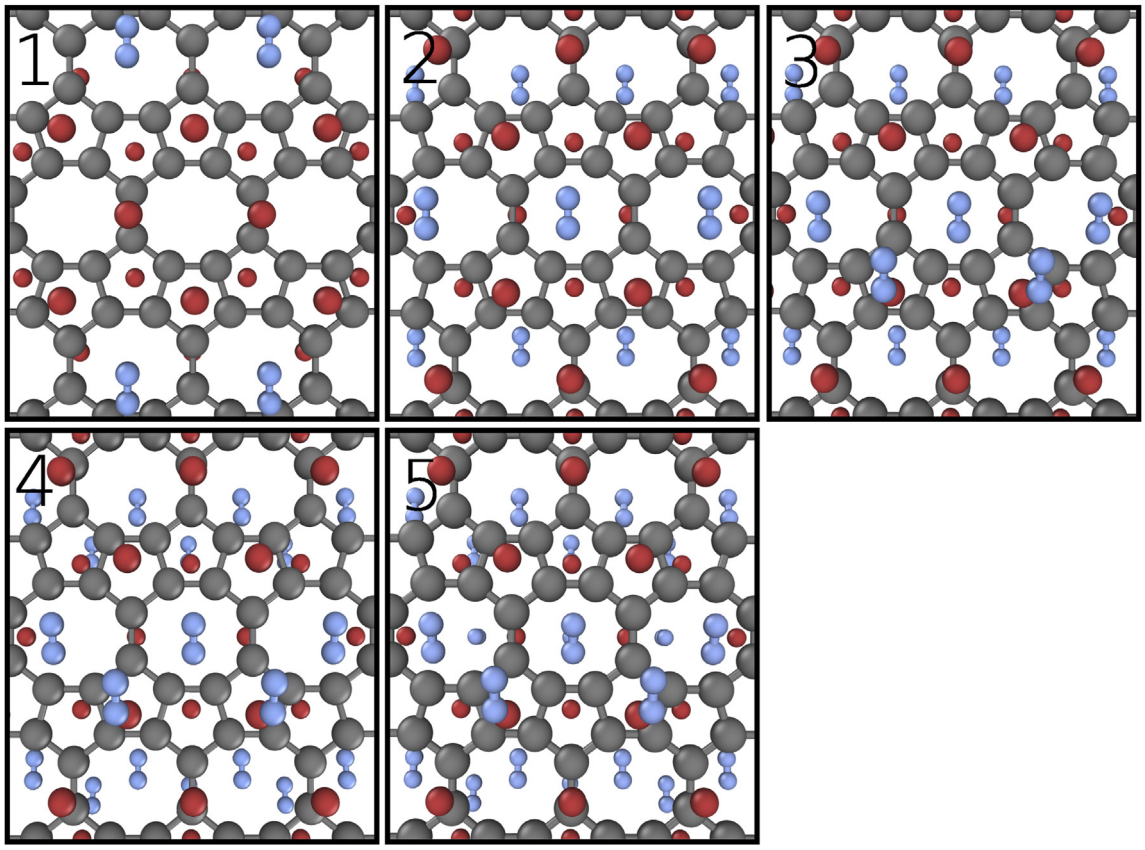

Fig. 7 – The most stable structures of the systems 6Li/PG + nH_2 ($n = 1$–5). The C, Li and H atoms are plotted as dark grey balls, red balls and small light blue balls, respectively. The Li and H atoms on the front side have a greater size than the Li and H atoms on the rear side. (For interpretation of the references to color in this figure legend, the reader is referred to the Web version of this article.)

[55] finds 32 BCPs connecting a Li atom to a C atom, whereas only 4 BCPs associated to the Li–Li bond are detected. The value of the electronic density at the BCPs of the Li–C bonding (see Table 1) is typical of an ionic bond ($\approx 0.02 - 0.03$ a.u.). The Li–Li interaction is twice weaker than the Li–C interaction. However, the stable structure (lower panels of Fig. 8) displays a smaller number of Li–C bonds (16), but a much higher number of Li–Li bonds (30). This result indicates that the latter structure corresponds to a strong bonding network. Moreover, the Li–Li bonding is a stabilizing contribution to the energy as demonstrated by the negative value of the energies at the BCPs. The larger number of bonds in the second structure supports the finding that it is more stable.

Successive decorations of popgraphene by Li atoms and H_2 molecules

Fig. 9 shows the results of our chemical topological analysis for the following systems (from left to right): pristine popgraphene, the (replicated) system 6Li/PG, and the system 6Li/PG + $4H_2$ (i.e., 6Li/PG saturated with four H_2 molecules). In the leftmost panel of Fig. 9, both BCPs and RCPs are shown, but the latter are not plotted for the other two structures for the sake of clarity. However, the behaviour after decorating the popgraphene structure with Li atoms and subsequently with H_2 molecules can be seen in the results listed in Table 2 for the RCPs and in Table 3 for the BCPs.

The side view of the pristine popgraphene structure (left-hand upper panel of Fig. 9) displays the planar geometry derived from the aromatic cycles. The electronic density and energies at the RCPs (Table 2) are indicative of the strength of the aromatic effect. It is pronounced for the pentagonal rings of popgraphene, where a value of 0.042 a.u. is found. This is superior to the value of 0.025 a.u. obtained for benzene complexes [48]. The electronic density at the RCPs for the pentagonal rings of popgraphene is almost one order of magnitude higher than that of the octagonal rings. The BCPs between C atoms depend of the C atom involved. The shorter the C–C bonds the stronger the density at the BCP. The C–C bonds are always covalent since the Laplacian of the electron density is highly negative (≈ -0.7 a.u.).

The addition of Li atoms on both sides of the popgraphene sheet leads to the appearance of new BCPs. In the middle panels of Fig. 9, these BCPs are plotted with green balls for Li–C bondings, and with yellow balls for Li–Li bondings. The most striking feature is the large number of BCPs joining the Li and C atoms. As it can be seen in Table 3, the bonding between the Li atoms and the C atoms of the popgraphene sheet is more intense than the Li–Li bonding. For instance, the BCP value of the electronic density for the Li–C bondings amounts

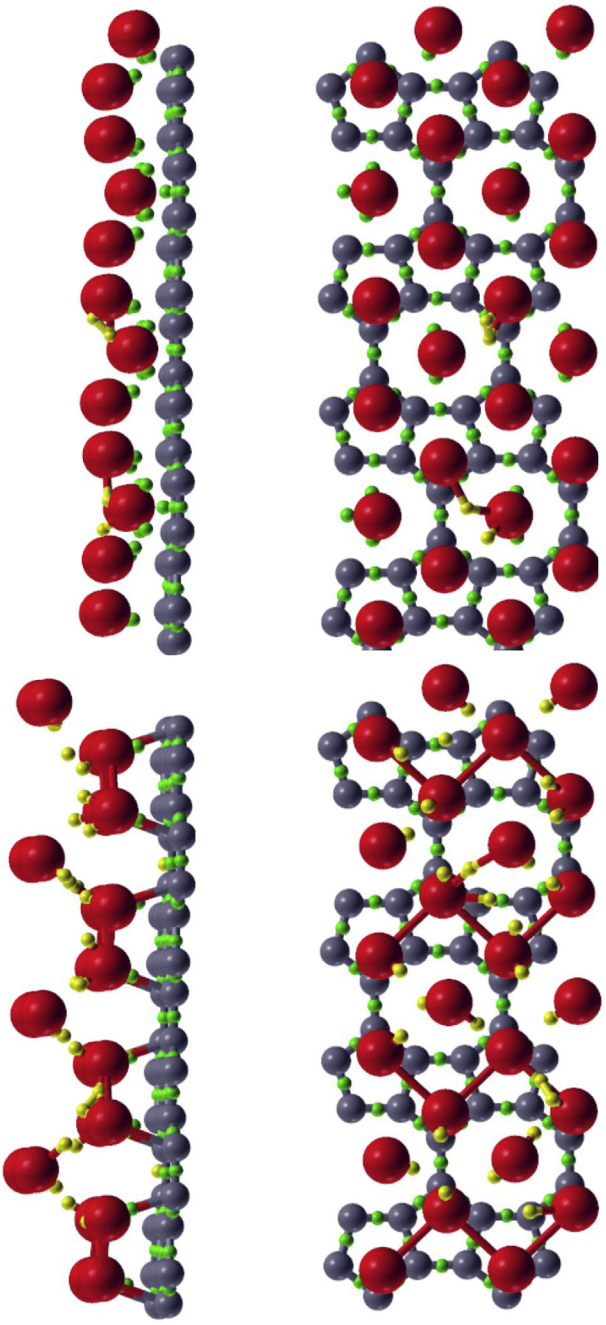

Fig. 8 – Side and top views of the metastable and stable Li-decorated popgraphene structures shown in Fig. 3. The C and Li atoms are plotted as dark grey balls and red balls, respectively. The bond critical points are represented with small yellow balls (Li–Li bonds) and green balls (Li–C bonds). (For interpretation of the references to color in this figure legend, the reader is referred to the Web version of this article.)

to about 0.020 a.u., while for the Li–Li interaction it is 0.006 a.u. The higher value of the BCP for the Li–C bonding amounts to 0.030 a.u. (the value corresponding to the C–C covalent bond is 0.270 a.u). This suggests an ionic contribution, which is confirmed by the positive values (≈0.2 a.u.) of the Laplacian and the slightly positive energy at the BCP [52]. Indeed, the

Table 1 – Average electronic density (ρ) and electronic energy (η) at the bond critical points for the Li–C and Li–Li bonds corresponding to the metastable and stable Li-decorated popgraphene structures shown in Fig. 3. Standard deviations are given in parenthesis. The results are in 10^{-3} a.u. (see the Computational details and theoretical background section).

Structure	Li–C	Li–Li	ρ_{Li-C}	η_{Li-C}	ρ_{Li-Li}	η_{Li-Li}
Metastable	32	4	22 (3)	3 (1)	10 (1)	−1.5 (3)
Stable	16	30	26 (2)	4.7 (6)	9 (2)	−0.9 (4)

electronic population on the Li atoms amounts to 2.1 electrons, which corresponds to a +0.9 charge, i.e., the Li atoms are almost ionic entities. These results are consistent with those obtained in the previous section, which showed that in the decoration of popgraphene by Li atoms they have a clear tendency to be separated. In the process of decorating popgraphene with Li atoms on both sides of the sheet, the C–C bonding slightly softens from 0.27 a.u to 0.26 a.u. This feature is associated to a condensation of the charge at the RCPs.

After saturating the Li-decorated popgraphene sheet with H_2 molecules, new molecular and atomic interactions intervene (right-hand panels of Fig. 9). The popgraphene sheet hardly captures more electrons, as suggested by the behaviour of both RCPs and BCPs in the last columns of Tables 2 and 3 Indeed, no changes in the features of the C–C or Li–C bonds are noted. The results of Table 3 show that three weak interactions glue the H_2 molecules to the Li-decorated popgraphene. The H_2–C interactions are the stronger, followed in order of intensity by the H_2–H_2 and the H_2–Li interactions. All those interactions are five times weaker than the already weak ionic interaction between the Li atoms and the C atoms of popgraphene. According to the corresponding very weak values of both the electronic density and energy at the BCPs, those interactions might be considered as vdW-type interactions. This interpretation relies on the almost negligible energetic contribution obtained for those bonds at the BCPs, a signature of the vdW nature of the bonding [52]. For comparison, in Table 3 we show the characteristics of the bonding in the Ti-decorated graphene nanoribbon saturated with four H_2 molecules per Ti atom that was considered in Ref. [26], but now with results obtained using DGrid5.1 [55]. We first note that the higher the value of the BCP between two atoms the more intense the bonding interaction between these atoms. The value of the electronic density at the BCPs between a H_2 molecule and the Ti atom (0.041 a.u) is twenty times larger than the value of the BCPs between the H_2 molecules and the Li atoms (0.002 a.u). Additionally, the energy at the BCPs between the H_2 molecule and the Ti atom is negative. These features, together with a positive Laplacian at the BCPs of 0.12 a.u for the H_2–Ti interaction, are typical of a metallic bonding interaction [52]. This latter bonding is often referred to as a Kubas interaction [58,59]. The effect of the transition metal Ti is much stronger than the effect of the underlying graphene layer and than the interaction between H_2 molecules ($H_2 \cdots H_2$). In fact, the average value at the BCPs between H_2 and Ti atoms, 0.041 a.u., exceeds the values of the BCPs for the H_2-graphene bonding interaction and the $H_2 \cdots H_2$ bonding

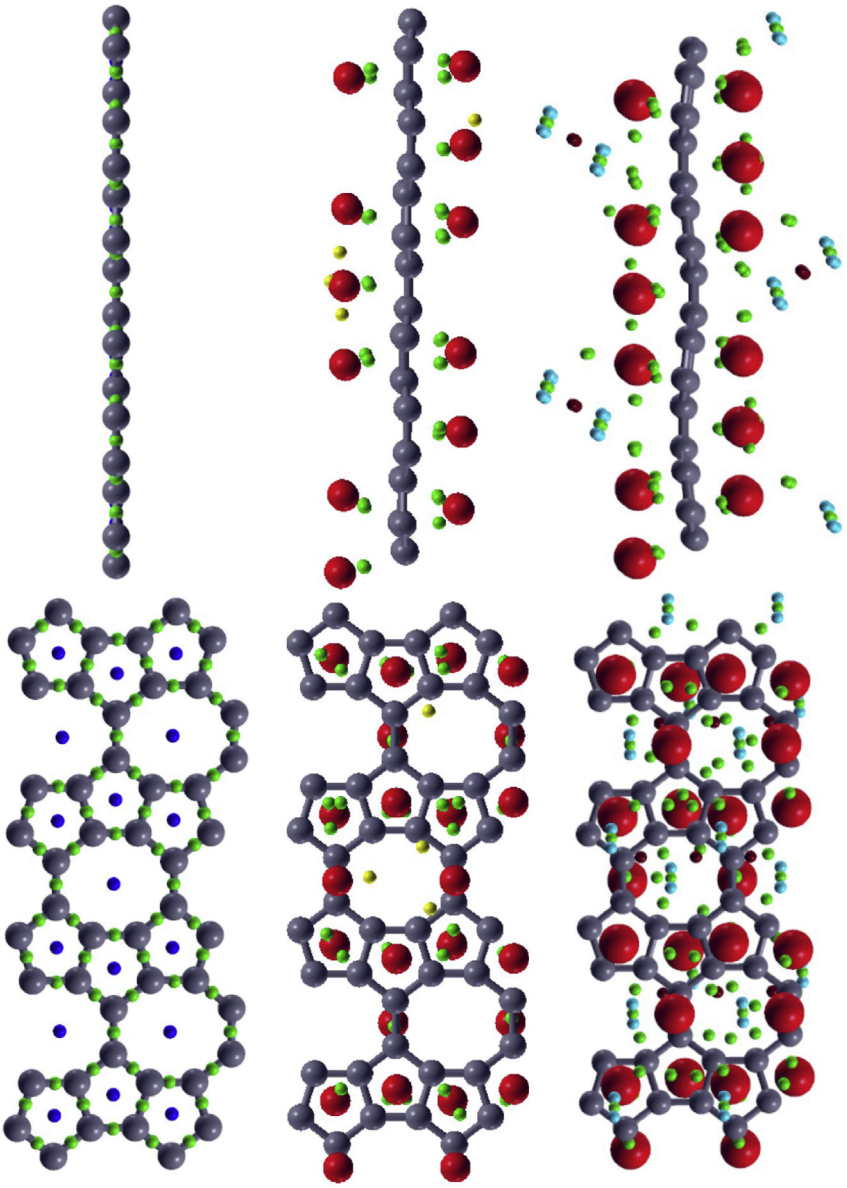

Fig. 9 – From left to right, side and top views of pristine popgraphene, popgraphene decorated with Li atoms on both sides of the sheet, and Li-decorated popgraphene with maximum H_2 uptake. The C, Li and H atoms are plotted as dark grey balls, red balls and small light blue balls, respectively. Bond critical points are represented with small green balls and ring critical points with dark blue balls, the latter only drawn for the pristine structure. Yellow small balls, only sketched in the middle panels, are bond critical points for in plane Li–Li bonds. Small purple balls denote molecular hydrogen bondings. (For interpretation of the references to color in this figure legend, the reader is referred to the Web version of this article.)

interaction, which are 0.0075 (5) a.u and 0.001 a.u., respectively. The metallic interaction of the transition metal atom with the H_2 molecules causes an elongation of the molecule, whose H–H distance is found to be 0.80 Å. Turning to the value of the density at the BCPs between the two H atoms, it is evidenced that the covalent bonding interaction has been weakened by the metallic interaction as it amounts to 0.200 a.u against 0.229 a.u. when the H_2 molecules undergo a bonding interaction with the Li atoms (see the corresponding lines in Table 3). Coming back to the system 6Li/PG + $4H_2$, we must point out that the results are not unexpected: the Li atoms have engaged their single valence 2s electron in the bonding with the C atoms of the popgraphene layer, the H atoms share their electrons in the H_2 molecules and the molecules are closed shell entities (the popgraphene layer is saturated with electrons). Thus, the H–H distance of the adsorbed H_2 molecule (0.76 Å) is hardly superior to that of the free H_2 molecule (0.74 Å). This cannot be termed as a Kubas-type interaction implying a σ^* orbital. The above analysis indicates, therefore, that in the systems 6Li/PG + $4H_2$ there are several interconnected closed shell interactions between electron clouds of weak intensity.

The global picture derived from our quantum chemical topological analysis of the system 6Li/PG + $4H_2$ is that the

Table 2 – Electronic densities at the ring critical points for the structures shown in the left (L), middle (M) and right (R) panels of Fig. 9. Standard deviation are given in parenthesis. The results are in 10^{-3} a.u. (see the Computational details and theoretical background section).

	L	M	R
Pentagon	42 (2)	45 (2)	45 (2)
Octagon	6.4 (7)	6.6 (4)	6.6 (3)

Table 3 – Electronic densities and energies at the bond critical points for the structures shown in the left (L), middle (M) and right (R) panels of Fig. 9 for selected types of bonds. The first values correspond to the electronic densities, always positive, and the second values to the energies. Standard deviations are given in parenthesis. For comparison, the values for the H–H and H_2–Ti bonds corresponding to an H_2 saturated Ti-decorated zigzag graphene nanoribbon are given in the last two rows (see text). The results are given in 10^{-3} a.u. (see the Computational details and theoretical background section), while the bond distances are in Å.

	Bond distance	L	M	R
C–C	1.40	292(2)/-315(5)	269(1)/-275(3)	269(1)/-275(3)
	1.44	275(9)/-281(2)	260(2)/-261(4)	260(2)/-261(4)
	1.46	267(1)/-269(1)	262(1)/-263(2)	260(1)/-259(2)
Li–C	1.88–2.25	–	20(10)/6(1)	22(2)/6(1)
Li–Li	3.11	–	5.5(7)/-0.5(1)	6.2(2)/0.6(2)
H–H	0.76	–	–	229(2)/-159(2)
$H_2 \cdots$ Li	3.10	–	–	2(1)/-0(0)
$H_2 \cdots$ C	3.40	–	–	4(1)/0.6(1)
$H_2 \cdots H_2$	3.00	–	–	3.0(4)/0.4(1)
H–H	0.80	–	–	200(6)/-133(5)
$H_2 \cdots$ Ti	1.95	–	–	41(3)/-8(4)

stabilization of the H_2 molecules comes from three weak contributions: the interaction of the molecules with both the Li and C atoms together with the interaction between the H_2 molecules.

Conclusions

In this work, we have performed vdW-corrected DFT calculations to investigate the adsorption of H_2 molecules on popgraphene, a recently proposed (and experimentally suggested) 2D carbon allotrope consisting in pentagonal-octagonal-pentagonal carbon rings forming a planar network. For this purpose, we decorated the popgraphene surface with Li atoms, which assist to the H_2 adsorption. The advantages of this element are multiple: it is light, it hardly modifies the popgraphene layer and it has no clustering tendency on that substrate.

Our calculations show that popgraphene can be decorated in a very stable way by placing the Li atoms on pentagonal hollow sites of both sides of the sheet, leaving free the octagonal hollow sites. This configuration, which contrasts with that proposed recently for Li/popgraphene [39], allows to reduce the Coulomb interactions between the Li atoms, which have transferred part of their charge to the popgraphene sheet. Diffusion analysis gives further support to the marked stability of the Li/popgraphene structure. The hybrid Li/popgraphene system can bind up to four H_2 molecules per unit cell (two for each side), with an average H_2-adsorption energy of 0.11 eV; this amounts to an efficient gravimetric density of 4.24 wt%.

The results inferred from our quantum-chemical topological analysis account for the nature of the bondings between the different atoms and molecules implied in the Li/popgraphene and Li/popgraphene + H_2 systems. In the stabilization of both systems, the most important role is played by the ionic interaction between the Li atoms and the C atoms of popgraphene: the Li atoms donate on average 0.9 electrons to the popgraphene layer, thus inducing Coulomb repulsions between them. The stabilization of the H_2 molecules in the hydrogenated system comes from three weak closed shell interactions, which imply both the H_2 molecules and the Li and C atoms.

Finally, we would like to point out that although our prediction for the hydrogen gravimetric density for Li-decorated popgraphene is a little below the DOE threshold, it could be probably be increased in real conditions, i.e., under appropriated pressures and/or temperatures. Therefore, Li-decorated popgraphene nanostructures could be promising materials for hydrogen storage.

Declaration of competing interest

The authors declare that they have no known competing financial interests or personal relationships that could have appeared to influence the work reported in this paper.

Acknowledgments

The financial support of the Spanish Ministry of Economy and Competitiveness (Grant PGC2018-093745-B-I00) is gratefully acknowledged. Moreover, this work was founded by the Junta de Castilla y León (Project No. VA124G18), the University of Valladolid, Spain, and the Xunta de Galicia (ED431E 2018/08, GRC ED431C 2016/001 and GRC ED431C 2020/10). Facilities provided by the Pole de Calcul Intensif pour la Mer (DATARMOR, Brest) are also acknowledged.

Appendix A. Supplementary data

Supplementary data to this article can be found online at https://doi.org/10.1016/j.ijhydene.2021.02.058.

REFERENCES

[1] Barreto L, Makihira A, Riahi K. The hydrogen economy in the 21st century: a sustainable development scenario. Int J Hydrogen Energy 2003;28(3):267–84.

[2] Crabtree GW, Dresselhaus MS, Buchanan MV. The hydrogen economy. Phys Today 2004;57(12):39–44.
[3] Marbán G, Valdés-Solís T. Towards the hydrogen economy? Int J Hydrogen Energy 2007;32(12):1625–37.
[4] Muradov NZ, Veziroğlu TN. 'Green' path from fossil-based to hydrogen economy: an overview of carbon-neutral technologies. Int J Hydrogen Energy 2008;33(23):6804–39.
[5] Ball M, Weeda M. The hydrogen economy-vision or reality? Int J Hydrogen Energy 2015;40(25):7903–19.
[6] Abe JO, Popoola A, Ajenifuja E, Popoola O. Hydrogen energy, economy and storage: review and recommendation. Int J Hydrogen Energy 2019;44(29):15072–86.
[7] Ren X, Dong L, Xu D, Hu B. Challenges towards hydrogen economy in China. Int J Hydrogen Energy 2020;45(59):34326–45.
[8] Lee SM, Lee YH. Hydrogen storage in single-walled carbon nanotubes. Appl Phys Lett 2000;76(20):2877–9.
[9] Zhao JJ, Buldum A, Han J, Lu JP. Gas molecule adsorption in carbon nanotubes and nanotube bundles. Nanotech 2002;13(2):195–200.
[10] Arellano JS, Molina LM, Rubio A, Alonso JA. Density functional study of adsorption of molecular hydrogen on graphene layers. J Chem Phys 2000;112(18):8114–9.
[11] Boukhvalov D, Katsnelson M, Lichtenstein A. Hydrogen on graphene: electronic structure, total energy, structural distortions and magnetism from first-principles calculations. Phys Rev B 2008;77(3):035427.
[12] Dimitrakakis GK, Tylianakis E, Froudakis GE. Pillared graphene: a new 3-D network nanostructure for enhanced hydrogen storage. Nano Lett 2008;8(10):3166–70.
[13] Ozturk Z, Baykasoglu C, Kirca M. Sandwiched graphene-fullerene composite: a novel 3-D nanostructured material for hydrogen storage. Int J Hydrogen Energy 2016;41(15):6403–11.
[14] Cabria I, López MJ, Alonso JA. Simulation of the hydrogen storage in nanoporous carbons with different pore shapes. Int J Hydrogen Energy 2011;36(17):10748–59.
[15] Jordá-Beneyto M, Suárez-García F, Lozano-Castelló D, Cazorla-Amorós D, Linares-Solano A. Hydrogen storage on chemically activated carbons and carbon nanomaterials at high pressures. Carbon 2007;45(2):293–303.
[16] Dash RK, Yushin G, Gogotsi Y. Synthesis, structure and porosity analysis of microporous and mesoporous carbon derived from zirconium carbide. Microporous Mesoporous Mater 2005;86(1–3):50–7.
[17] Dillon AC, Jones KM, Bekkedahl TA, Kiang CH, Bethune DS, Heben MJ. Storage of hydrogen in single-walled carbon nanotubes. Nature 1997;386(6623):377–9.
[18] Kostoglou N, Constantinides G, Charalambopoulou G, Steriotis T, Polychronopoulou K, Li Y, et al. Nanoporous spongy graphene: potential applications for hydrogen adsorption and selective gas separation. Thin Solid Films 2015;596:242–9.
[19] Kostoglou N, Tarat A, Walters I, Ryzhkov V, Tampaxis C, Charalambopoulou G, et al. Few-layer graphene-like flakes derived by plasma treatment: a potential material for hydrogen adsorption and storage. Microporous Mesoporous Mater 2016;225:482–7.
[20] Kostoglou N, Koczwara C, Prehal C, Terziyska V, Babic B, Matovic B, et al. Nanoporous activated carbon cloth as a versatile material for hydrogen adsorption, selective gas separation and electrochemical energy storage. Nanomater Energy 2017;40:49–64.
[21] Office of energy efficiency & renewable energy, fuel cell technologies office, materials-based hydrogen storage. 2018. URL: https://www.energy.gov/eere/fuelcells/materials-based-hydrogen-storage. [Accessed 26 February 2020].
[22] Office of energy efficiency & renewable energy, fuel cell technologies office, DOE technical targets for onboard hydrogen storage for light-duty vehicles. 2018. URL: https://www.energy.gov/eere/fuelcells/doe-technical-targets-onboard-hyd rogen-storage-light-duty-vehicles. [Accessed 26 February 2020].
[23] Bhatia SK, Myers AL. Optimum conditions for adsorptive storage. Langmuir 2006;22(4):1688–700.
[24] Li J, Furuta T, Goto H, Ohashi T, Fujiwara Y, Yip S. Theoretical evaluation of hydrogen storage capacity in pure carbon nanostructures. J Chem Phys 2003;119(4):2376–85.
[25] Yildirim T, Ciraci S. Titanium-decorated carbon nanotubes as a potential high-capacity hydrogen storage medium. Phys Rev Lett 2005;94(17):175501.
[26] Lebon A, Carrete J, Gallego LJ, Vega A. Ti-decorated zigzag graphene nanoribbons for hydrogen storage. A van der Waals-corrected density-functional study. Int J Hydrogen Energy 2015;40(14):4960–8.
[27] Li QF, Wan XG, Duan CG, Kuo JL. Theoretical prediction of hydrogen storage on Li-decorated monolayer black phosphorus. J Phys D Appl Phys 2014;47(46):465302.
[28] Yu ZY, Wan N, Lei SY, Yu H. Enhanced hydrogen storage by using lithium decoration on phosphorene. J Appl Phys 2016;120(2):024305.
[29] Haldar S, Mukherjee S, Ahmed F, Singh CV. A first principles study of hydrogen storage in lithium decorated defective phosphorene. Int J Hydrogen Energy 2017;42(36):23018–27.
[30] Garara M, Benzidi H, Lakhal M, Louilidi M, Ez-Zahraouy H, El Kenz A, et al. Phosphorene: a promising candidate for H_2 storage at room temperature. Int J Hydrogen Energy 2019;44(45):24829–38.
[31] Er S, de Wijs GA, Brocks G. DFT study of planar boron sheets: a new template for hydrogen storage. J Phys Chem C 2009;113(43):18962–7.
[32] Li L, Zhang H, Cheng X. The high hydrogen storage capacities of li-decorated borophene. Comp Mat Sci 2017;137:119–24.
[33] Lebon A, Aguilera del Toro RH, Gallego LJ, Vega A. Li-decorated pmmn8 phase of borophene for hydrogen storage. A van der Waals corrected density-functional theory study. Int J Hydrogen Energy 2019;44(2):1021–33.
[34] Joseph J, Sivasankarapillai VS, Nikazar S, Shanawaz MS, Rahdar A, Lin H, et al. Borophene and boron fullerene materials in hydrogen storage: opportunities and challenges. ChemSusChem 2020;13(15):3754–65.
[35] Zhang SH, Zhou J, Wang Q, Chen XS, Kawazoe Y, Jena P. Penta-graphene: a new carbon allotrope. Proc Natl Acad Sci Unit States Am 2015;112(8):2372–7.
[36] Wang Z, Zhou XF, Zhang X, Zhu Q, Dong H, Zhao M, et al. Phagraphene: a low-energy graphene allotrope composed of 5–6–7 carbon rings with distorted Dirac cones. Nano Lett 2015;15(9):6182–6.
[37] Li X, Wang Q, Jena P. ψ-graphene: a new metallic allotrope of planar carbon with potential applications as anode materials for lithium-ion batteries. J Phys Chem Lett 2017;8(14):3234–41.
[38] Fan X, Li J, Chen G. New carbon allotropes with metallic conducting properties: a first-principles prediction. RSC Adv 2017;7(28):17417–26.
[39] Wang S, Yang B, Chen H, Ruckenstein E. Popgraphene: a new 2D planar carbon allotrope composed of 5–8–5 carbon rings for high-performance lithium-ion battery anodes from bottom-up programming. J Mater Chem A 2018;6(16):6815–21.
[40] Chen JH, Autès G, Alem N, Gargiulo F, Gautam A, Linck M, et al. Controlled growth of a line defect in graphene and implications for gate-tunable valley filtering. Phys Rev B 2014;89(12):121407.
[41] Kresse G, Hafner J. Ab initio molecular-dynamics for liquid metals. Phys Rev B 1993;47(1):558.

[42] Kresse G, Furthmüller J. Efficient iterative schemes for ab initio total-energy calculations using a plane-wave basis set. Phys Rev B 1996;54(16):11169.
[43] Perdew JP, Burke K, Ernzerhof M. Generalized gradient approximation made simple. Phys Rev Lett 1996;77(18):3865.
[44] Grimme S. Semiempirical GGA-type density functional constructed with a long-range dispersion correction. J Comput Chem 2006;27(15):1787–99.
[45] Blöchl PE. Projector augmented-wave method. Phys Rev B 1994;50(24):17953.
[46] Methfessel M, Paxton AT. High-precision sampling for brillouin-zone integration in metals. Phys Rev B 1989;40(6):3616.
[47] Becke AD, Edgecombe KE. A simple measure of electron localization in atomic and molecular-systems. J Chem Phys 1990;92(9):5397–403.
[48] Lebon A, Orain PY, Memboeuf A. Understanding the CO dissociation in $[Fe(CN)_2(CO)_2$ (dithiolate)$]^{2-}$ complexes with quantum chemical topology tools. J Phys Chem 2017;121(37):7031–41.
[49] Palusiak M, Krygowski TM. Application of AIM parameters at ring critical points for estimation of π-electron delocalization in six-membered aromatic and quasi-aromatic rings. Chem–A European J 2007;13(28):7996–8006.
[50] Falkowska E, Tognetti V, Joubert L, Jubault P, Bouillon JP, Pannecoucke X. First efficient synthesis of SF_5-substituted pyrrolidines using 1,3-dipolar cycloaddition of azomethine ylides with pentafluorosulfanyl-substituted acrylic esters and amides. RSC Adv 2015;5(9):6864–8.
[51] Popelier P. Atoms in molecules: an introduction. London: Prentice Hall; 2000.
[52] Matta CF. Hydrogen–hydrogen bonding: the non-electrostatic limit of closed-shell interaction between two hydro. Dordrecht: Springer Netherlands; 2006. p. 337–75.
[53] Frisch MJ, Trucks GW, Schlegel HB, Scuseria GE, Robb MA, Cheeseman JR, et al. Gaussian 16 revision C.01. Wallingford CT: Gaussian Inc; 2016.
[54] Otero-de-la Roza A, Johnson ER, Luaña V. CRITIC2: A program for real-space analysis of quantum chemical interactions in solids. Comput Phys Commun 2014;185(3):1007–18.
[55] Kohout M. Dgrid. Version 51, Dresden. 2019. URL: https://www2.cpfs.mpg.de/kohout/Documents/dgrid-html/dgrid.html.
[56] Chan KT, Neaton JB, Cohen ML. First-principles study of metal adatom adsorption on graphene. Phys Rev B 2008;77(23):235430.
[57] Nakada K, Ishii A. Migration of adatom adsorption on graphene using DFT calculation. Solid State Commun 2011;151(1):13–6.
[58] Kubas GJ, Ryan RR, Swanson BI, Vergamini PJ, Wasserman HJ. Characterization of the first examples of isolable molecular hydrogen complexes, M(CO)3(PR3)2(H2)(M = Molybdenum or Tungsten; R = Cy or isopropyl). Evidence for a side-on bonded dihydrogen ligand. J Am Chem Soc 1984;106(2):451–2.
[59] Skipper CV, Hamaed A, Antonelli DM, Kaltsoyannis N. The Kubas interaction in M(II)(M = Ti, V, Cr) hydrazine-based hydrogen storage materials: a DFT study. Dalton Trans 2012;41(28):8515–23.